Nucleic Acids Research, 2026, **54**, gkag436
https://doi.org/10.1093/nar/gkag436
Nucleic Acid Enzymes

A universal and orthogonal safety valve for CRISPR/Cas12a without chemical modification or external stimulation

Wang Luo[1,†], You Wu[1,2,†], Dongsheng Ni[1,†], Li Zhang[1,2,†], Yiqi Zhang[2], Xiaole Han[2], Yaoyi Zhang[2], Jiu Pu[2], Yu He[2], Na Yin[2], Weitao Wang[2], Rongzhong Huang[1], Yongcan Guo[1,3,*], Yang Sun[4,*], Guoming Xie[1,2,*]

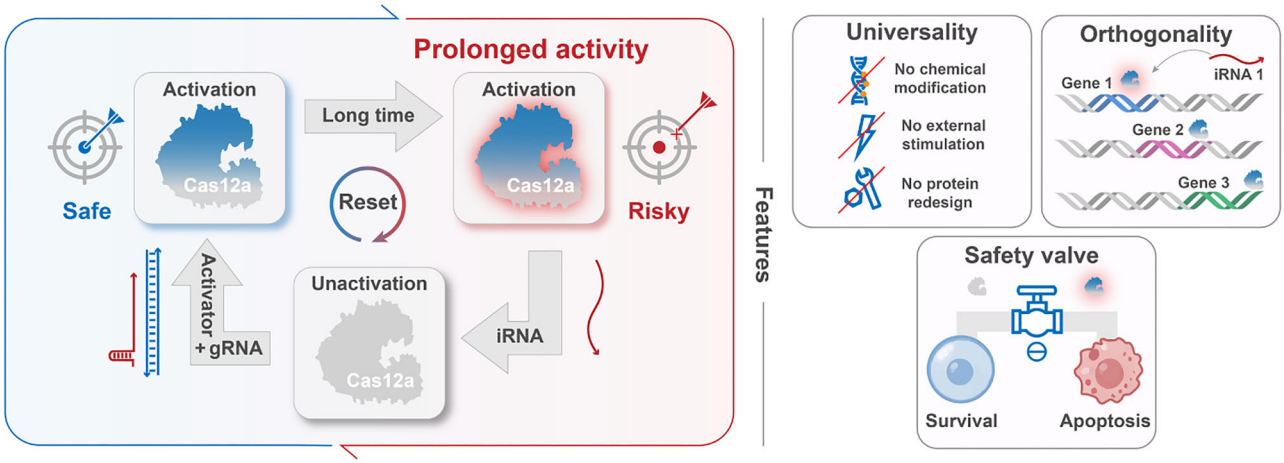
[1]Precision Medicine Center, Gut Microbiome Diagnosis and Treatment Center, Chongqing Municipality Clinical Research Center for Geriatrics and Gerontology, The Second Affiliated Hospital of Chongqing Medical University, Chongqing 400010, PR China
[2]Key Laboratory of Clinical Laboratory Diagnostics (Chinese Ministry of Education), College of Laboratory Medicine, Chongqing Medical Laboratory Microfluidics and SPRi Engineering Research Center, Chongqing Medical University, Chongqing 400016, PR China
[3]Clinical Laboratory of Traditional Chinese Medicine Hospital Affiliated to Southwest Medical University, Luzhou 646000, PR China
[4]Department of Ultrasound, Chongqing Key Laboratory of Ultrasound Molecular Imaging, the Second Affiliated Hospital of Chongqing Medical University, Chongqing 400010, PR China

*To whom correspondence should be addressed. Email: swtcmlab@163.com
Correspondence may also be addressed to Yang Sun. Email: sunyang@cqmu.edu.cn
Correspondence may also be addressed to Guoming Xie. Email: guomingxie@cqmu.edu.cn
†These authors contributed equally to this work.

Abstract

CRISPR/Cas-based gene editing technologies have achieved remarkable progress over the past decade, yet their broad practical applications remain limited by safety concerns. Although regulatory strategies applied before or during CRISPR/Cas activation have substantially improved sequence, temporal, and spatial specificity, persistent activity of already activated Cas nucleases may still increase the risk of uncontrolled editing. Therefore, an effective post-activation control strategy is urgently needed. Here, we report a modification- and stimulation-free RNA inhibitor (iRNA) that functions as a post-activation safety valve for CRISPR/Cas12a. By exploiting Cas12a's allosteric sensitivity and the thermodynamic and kinetic programmability of nucleic acid strand displacement, iRNA drives already activated Cas12a ribonucleoproteins back to an inactive state, enabling universal, sequence-programmable, and orthogonal post-activation inhibition within the validated Cas12a framework. Experiments and simulations elucidate the mechanistic basis of iRNA-mediated strand displacement and demonstrate its high inhibitory efficiency, reversible cyclic control, compatibility, expandability, orthogonality, and universality. Importantly, iRNA also acts as a programmable, autonomously operating safety valve in cells, suppressing uncontrolled editing while preserving PCSK9 gene knockout. With its simple design, excellent biocompatibility, and autonomous intracellular expression, iRNA provides a foundation for next-generation controllable CRISPR systems and holds broad potential for precision therapeutics, cell therapy, and molecular diagnostics.

Graphical abstract



Received: February 26, 2026. **Revised:** April 15, 2026. **Accepted:** April 16, 2026
© The Author(s) 2026. Published by Oxford University Press.
This is an Open Access article distributed under the terms of the Creative Commons Attribution-NonCommercial License (https://creativecommons.org/licenses/by-nc/4.0/), which permits non-commercial re-use, distribution, and reproduction in any medium, provided the original work is properly cited. For commercial re-use, please contact reprints@oup.com for reprints and translation rights for reprints. All other permissions can be obtained through our RightsLink service via the Permissions link on the article page on our site—for further information please contact journals.permissions@oup.com.

Downloaded from https://academic.oup.com/nar/article/54/8/gkag436/8666736 by guest on 05 May 2026

Introduction

The CRISPR system consists of a nucleic acid component, the gRNA (or crRNA), and a protein component, the Cas nuclease. Owing to its efficient and programmable sequence-recognition and cleavage capabilities, it has become a core tool in genome editing and molecular diagnostics [1, 2]. Over the past decade, continuous breakthroughs have been achieved in expanding CRISPR performance, including improving editing efficiency, enhancing detection sensitivity, overcoming PAM restrictions, and increasing multifunctionality and target flexibility [3–5]. However, as applications deepen, safety issues have gradually become one of the primary obstacles limiting the clinical translation and long-term use of CRISPR [4–11].

Current CRISPR systems still face challenges such as off-target editing, undesired chromosomal translocations, and genomic toxicity [3–14]. To address these issues, extensive research has focused on enhancing sequence, temporal, and spatial specificity before or during CRISPR activation (pre-activation or competitive-activation). For example, engineering Cas nucleases through protein engineering [15–18], regulating gRNA through structural interference [19–24] or chemical modifications [14, 25–28], can effectively reduce off-target reactions. Material encapsulation or steric-hindrance strategies combined with stimulus-responsive modules (such as light, sound, temperature, pH, enzymes, or chemical reagents [29–41]) can also keep CRISPR activity closed prior to activation and precisely trigger it under external stimulation. Although these strategies have substantially improved CRISPR safety, the risk of loss of control is not limited to the pre-activation or co-activation stages: the prolonged high activity of CRISPR after activation (post-activation) is also a significant safety hazard [6, 7, 42].

As illustrated in Scheme 1A, even if the CRISPR/Cas system can accurately cleave the target sequence at the initial stage (the validity period), its prolonged high activity may still gradually accumulate off-target cleavage and cut similar sequences (the risk period), leading to safety issues in gene editing and reduced specificity in molecular diagnostics. Therefore, establishing a post-activation control mechanism for CRISPR is essential. Such a mechanism, acting as a safety valve, could provide a "rapid shut-off" when CRISPR becomes uncontrolled and causes severe adverse effects (e.g. cytokine storm), thereby effectively preventing off-target activity and cytotoxicity (Scheme 1B).

Post-activation inhibition (Post-AI) of CRISPR can be achieved by regulating the half-life of Cas proteins, but large fused regulatory domains may be difficult to deliver and may reduce editing efficiency; moreover, additional regulatory domains may introduce undesired genomic alterations or transcriptomic perturbations, raising biosafety concerns in therapeutic gene editing [6, 7, 11]. Disrupting gRNA function through chemical modifications or external stimuli can also initiate and terminate CRISPR reactions, but such strategies often require case-by-case redesign and may therefore suffer from limited universality, poor flexibility, and difficulties in broad adaptation across different sequence contexts. Even when combining multiple chemical modifications or different wavelengths of light, the diversity of CRISPR editors that can be simultaneously controlled remains limited [29–41]. Protein-based anti-CRISPRs (Acr) or RNA-based anti-CRISPRs (rAcr) from bacteriophages and mobile genetic elements [6, 12, 15, 42–44] can bind CRISPR/Cas ribonucleoproteins (RNPs) and inhibit their function, but these inhibitors may introduce immunogenicity, exhibit insufficient selectivity, display poor orthogonality, and possess limited Post-AI efficiency. In summary, Post-AI remains the weakest and least resolved link in CRISPR safety regulation.

Recent studies, including our previous work, have shown that nucleic acid strand displacement reactions can accurately and broadly tune CRISPR performance before or during activation [13, 45–49], by imposing stricter hybridization conditions between the target and gRNA to reduce nonspecific reactions. However, once activated, CRISPR complexes possess high structural stability and substantial energetic barriers; conventional strand displacement cannot effectively reverse the activated conformation. Therefore, achieving Post-AI requires an entirely new regulatory and design logic.

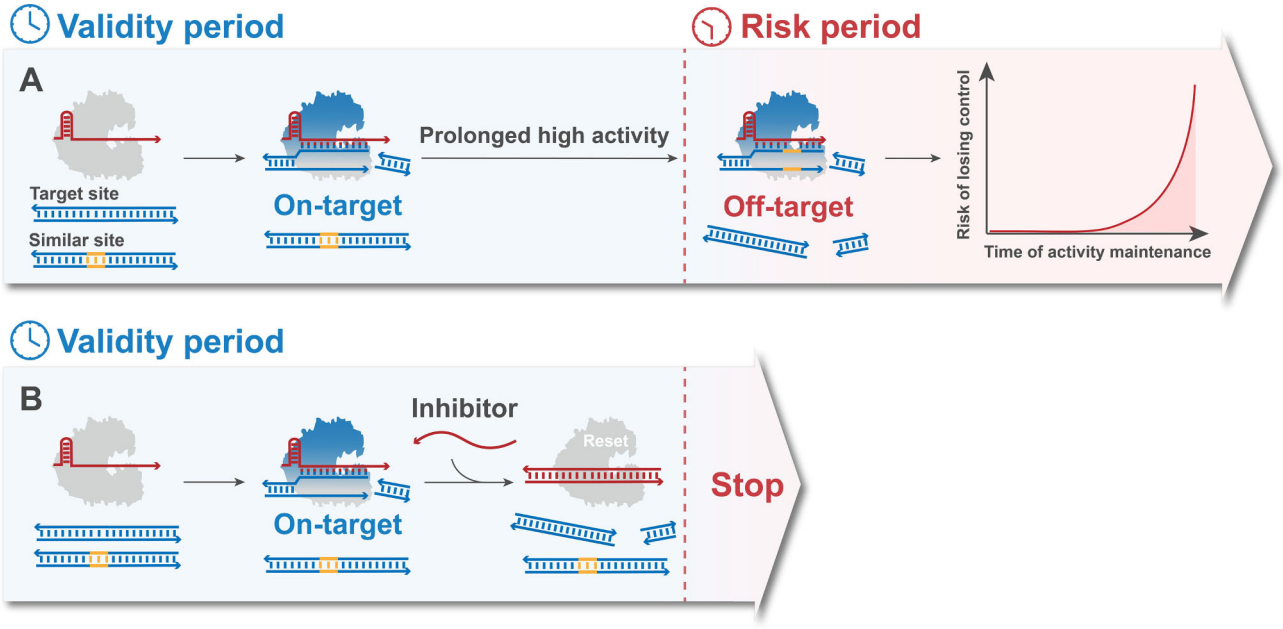
Based on this, the present study proposes a chemical-modification-free and external-stimulation-free RNA inhibitor (iRNA) that leverages the allosteric sensitivity of Cas12a and, under the thermodynamic and kinetic drive of nucleic acid strand displacement, effectively restores activated Cas12a RNPs to the unactivated state (Scheme 1B), achieving efficient and reversible Post-AI of the CRISPR system. Through systematic experiments and simulations, we elucidate the theoretical mechanism of the iRNA strand displacement strategy and experimentally validate its high inhibition efficiency, cyclic activity control, compatibility and expandability, orthogonality, and universality. More importantly, we demonstrate at the cellular level that iRNA can serve as a programmable and automated safety valve for CRISPR genome editing: while halting uncontrolled editing and restoring cellular function, it enables safe knockout of the cardiovascular disease-related gene PCSK9 [50], thereby reducing cardiovascular disease risks. This short-RNA safety valve has simple design rules, good biocompatibility, and can even be autonomously generated inside cells through controllable transcription, offering potential for self-regulating intracellular safety circuits. Overall, it provides a foundation for next generation adaptive and controllable CRISPR systems and shows promising applications in precision medicine, cell therapy, and molecular diagnostics.

Materials and methods

Materials

EnGen®Lba Cas12a (Cpf1, 100 μM) and rCutSmartTM buffer (50 mM potassium acetate, 20 mM trisacetate, 10 mM magnesium acetate, 100 μg/mL recombinant albumin, pH 7.9) were purchased from New England Biolabs. RNA sequences, magnesium chloride hexahydrate ($MgCl_2$ $\cdot 6H_2O$) and TE buffer were obtained from Sangon Biotech Inc. (Shanghai, China). DNA sequences were synthesized by Tsingke Biotechnology Co., Ltd (Beijing, China). RNase If and Proteinase K were obtained from Titan Scientific Co., Ltd (Shanghai, China). Ten per cent fetal bovine serum and 1% penicillin/streptomycin were obtained from VivaCell, BIOSCIENCES (Shanghai, China). JetPRIME was obtained from Polyplus, Illkirch Graffenstaden (France, 101000046). BCA kit was obtained from Pierce, Walham (MA, USA). Anti-HA (1:10 000) and anti-GFP (1:5000) were obtained from Abclonal. Anti-PCSK9 (1:1000), and anti-β-Tubulin (1:5000) were obtained from Proteintech. Kit-8 (CCK-8) was obtained from, Zeheng, Chongqing (China, ZH0025). All chemical

Downloaded from https://academic.oup.com/nar/article/54/8/gkag436/8666736 by guest on 05 May 2026



Scheme 1. Post-activation loss-of-control risk and the concept of a safety valve. (**A**) The CRISPR/Cas system can accurately cleave target sequences during the initial activation period, but prolonged catalytic activity inevitably increases the risk of mistargeting to similar sequences, leading to loss-of-control events. (**B**) A post-activation safety-valve mechanism is designed to rapidly shut down CRISPR activity once undesired activation or toxicity occurs. All sequences in this study are shown in Supplementary Tables S1 and S2, and Supplementary Schemes S2–S15.

reagents were of analytical grade, and RNase-free water was used throughout this study. All sequences in this study are shown in Supplementary Tables S1 and S2 and Supplementary Schemes S2–S15.

Instrument

The real-time fluorescence curves and endpoint fluorescence were recorded by a RotorGene 6000 instrument (Corbett Research, Mortlake, Australia) in the yellow channel (excitation wavelength: 535 nm; emission wavelength: 556 nm), or the green channel (excitation wavelength: 490 nm; emission wavelength: 520 nm).

Methods

Preparing the CRISPR–Cas12a reaction

The Cas12a and gRNA were assembled by mixing them in nuclease-free water followed by incubation at room temperature for 30 min. The activation assay was conducted in a final volume of 20 μL, including 1× rCutSmart buffer, 20 nM Cas12a-gRNA complexes, 250 nM DNA reporter, 12.5 mmol/L TE-Mg^{2+} buffer and various concentrations of the activators.

CRISPR–Cas12a activity duration assay

Twenty-five nanomolar assembled Cas12a-gRNA complexes were divided into four incubation groups in 1× rCutSmart buffer and 12.5 mmol/L TE-Mg^{2+} buffer: (i) complexes coincubated with target at 37°C, (ii) complexes coincubated with target at 4°C, (iii) complexes incubated alone at 37°C, and (iv) complexes incubated alone at 4°C. All groups were incubated for 35 days. At 7-day intervals, 20 μL of incubation solution was collected from each group and added to a reaction system containing 250 nM DNA reporter. For the two groups with Cas12a-gRNA complexes incubated alone, 25 nM target was additionally supplemented before real-time fluorescence signal monitoring of all four groups.

CRISPR–Cas12a specificity assay

Twenty nanomolar Cas12a-gRNA complexes and 50 nM ds-DNA activator were incubated at 37°C, followed by 1× rCutSmartTM buffer, 12.5 mmol/L TE-Mg^{2+} buffer and 250 nM DNA reporter. The endpoint fluorescence signals of the reaction systems were detected by Rotor-Gene 6000 instrument at irregular intervals.

Discrimination factor formula

$$DF = ([F_{PM}] - \text{background}) / ([F_{MM}] - \text{background}).$$

For Pre-AI assay

gRNAs of different lengths were individually co-incubated with Cas12a to prepare Cas12a-gRNA complexes. Two-hundred nanomolar iRNAs of different lengths were incubated with 25 nM Cas12a-gRNA complexes at 37°C for 60 min. After incubation, 25 nM ds-activators, and 250 nM DNA reporter were added to the system to record fluorescence changes.

For Co-AI assay

Two-hundred nanomolar iRNAs of different lengths, 25 nM Cas12a-gRNA complexes, 25 nM ds-activators, and 250 nM DNA reporter were mixed directly, followed by real-time fluorescence signal detection.

For Post-AI assay

In a reaction system containing 1× rCutSmartTM buffer and 12.5 mmol/l TE-Mg^{2+} buffer, 25 nM Cas12a-gRNA complexes, 25 nM ds-activators, and 250 nM DNA reporter were

Downloaded from https://academic.oup.com/nar/article/54/8/gkag436/8666736 by guest on 05 May 2026

added to monitor real-time fluorescence signals. After complete reporter cleavage, 200 nM iRNA, another gRNA, or another handle was added to the system, followed by incubation at 37°C for 60 min. Subsequently, 250 nM DNA reporter was added again to monitor real-time fluorescence signals continuously.

Twenty-four-hour inhibition efficiency assay

Four-hundred nanomolar iRNAs of different lengths were incubated with 20 nM Cas12a-gRNA complexes in a system containing 1× rCutSmartTM buffer and 12.5 mmol/l TE-Mg^{2+} buffer for 60 min. Then, 25 nM activators were added, and the mixture was further incubated for 24 h. Subsequently, DNA reporter was added to the reaction system, followed by fluorescence signal monitoring.

Cyclic activity control assay

Briefly, the activation assay and inhibition experiments were conducted in accordance with the protocol detailed above. Upon completion of inhibition, 250 nM DNA reporter was added to monitor real-time fluorescence for 30 min. Subsequently, 250 nM Cas12a-gRNA complex and 100 nM ds-activators were added to monitor real-time fluorescence for 30 min. Thereafter, 800 nM iRNA was added and the mixture was incubated at 37°C for 60 min; following this incubation, 250 nM DNA reporter was re-added to monitor real-time fluorescence changes over 30 min. Finally, 400 nM Cas12a-gRNA complex and 100 nM ds-activators was supplemented, and the fluorescence signal emitted by the reactivated Cas12a-gRNA complex was continuously monitored.

Photocontrolled CRISPR–Cas12a inhibition assay

The iRNA was replaced with a PC-Linker-modified iRNA. The mixture was incubated at 37°C for 60 min, after which 250 nM DNA reporter was added to monitor real-time fluorescence for 30 min. Subsequently, the mixture was irradiated with a UV lamp (λ 365 nm, 35 W) for 5 min. Finally, real-time fluorescence changes were monitored.

Orthogonal inhibition experiment

The activation assay was carried out following the same protocol as mentioned above. After the activated Cas12a-gRNA complexes were treated with three independent parallel methods, 250 nM DNA reporter was added to each group respectively to continue monitoring real-time fluorescence signals. The specific treatments were detailed as follows: (i) 1 mg/ml proteinase K was added to the system to digest the Cas protein at 37°C for 15 min; (ii) the complexes were inactivated at 70°C; after cooling the temperature to 37°C, 5 U/ml RNase If was added to digest the gRNA for 15 min; finally, 20 nM Cas protein was added to the system; (iii) 200 nM different iRNAs were added to the system, followed by incubation at 37°C for 60 min.

Partial methods are detailed in the supplementary materials.

Results and discussion

Sustained activity and loss-of-control risk of CRISPR/Cas12a

After activation, the CRISPR/Cas12a RNP can maintain its activity for an extended period, which provides strong performance and efficiency, but this long half-life may also introduce potential safety hazards [6, 7, 42]. To investigate the stability of activated Cas12a RNPs and the duration of their retained activity, as shown in Fig. 1A and B, we incubated unactivated and activated Cas12a RNPs at 37°C for extended periods and dynamically measured their *trans*-cleavage activity. The unactivated Cas12a RNP showed a significant decrease in activity by day 7 (F 0.62) and almost no activity after day 14 (F 0.03). In contrast, the activated RNP exhibited almost no decline in activity even at day 35 (F 0.91). As a control, in Supplementary Fig. S1, when the incubation temperature was set at 4°C, both unactivated and activated RNPs maintained almost full activity (F 1.00) over 35 days. Further experiments (Supplementary Figs S2 and S3) showed that the loss of activity at 37°C was due to the sequential degradation of gRNA (14 days) and Cas12a nuclease (21 days). In Supplementary Fig. S4, we compared the effect of three gRNAs and a random RNA sequence on Cas12a stability in HepG2 cells; after 144 h, activated Cas12a RNPs were clearly preserved at higher levels. These results indicate that activated Cas12a RNPs possess markedly higher stability and retain activity for much longer periods, thereby creating a substantial potential for post-activation loss of control and helping explain the intrinsic difficulty of Post-AI.

Although numerous new technologies have been developed to improve the sequence, temporal, and spatial specificity of CRISPR [14–41], the risk of loss of control cannot be fully eliminated as long as Cas12a RNP activity persists for extended periods. As shown in Fig. 1C–F and Supplementary Figs S5 and S6, we introduced mismatches of different lengths (1/2/3 nt) at various positions within the target sequence (Mismatch-1/2/3/4) and assessed CRISPR/Cas12a specificity using fluorescence readouts. In all cases, specificity progressively declined as activation time increased, with most DFs dropping close to 1 after 200 min. Even for the 3 nt Mismatch-3 and Mismatch-4 groups, whose initial DFs reached 119.4 and 259.7, respectively, the DFs sharply decreased to 4.9 and 4.2 after 200 min. With further extension of reaction time, specificity eventually vanished entirely.

More stringent recognition strategies may improve CRISPR specificity, but over extended time windows they are more likely to delay, rather than prevent, the gradual loss of specificity. This time-dependent accumulation of loss-of-control risk arises from the intrinsic fuzzy-recognition and post-activation turnover properties of Cas proteins [3–14]. As shown in Fig. 1G–H, we labeled a double-stranded probe (ds-probe) with a fluorophore and quencher, whose fluorescence is produced only upon *cis*-cleavage. The results showed that unactivated Cas12a RNP generated fluorescence by fuzzy-recognition of the ds-probe (sequence similar to the target); activated Cas12a RNP (already bound to the target) could also bind the ds-probe (sequence similar to the target) through a turnover mechanism, generating fluorescence more rapidly. When the ds-probe sequence was completely dissimilar to the target, neither activated nor unactivated RNPs produced fluorescence, confirming that the ds-probe is cleaved only under fuzzy-recognition or turnover mechanisms.

Activated Cas12a RNPs exhibit significantly enhanced structural stability and extremely prolonged activity retention. Combined with their intrinsic fuzzy-recognition and turnover-cleavage properties, the risk of loss of control inevitably accumulates over time. Therefore, establishing a post-activation control mechanism for CRISPR is crucial. Such a safety valve

Downloaded from https://academic.oup.com/nar/article/54/8/gkag436/8666736 by guest on 05 May 2026

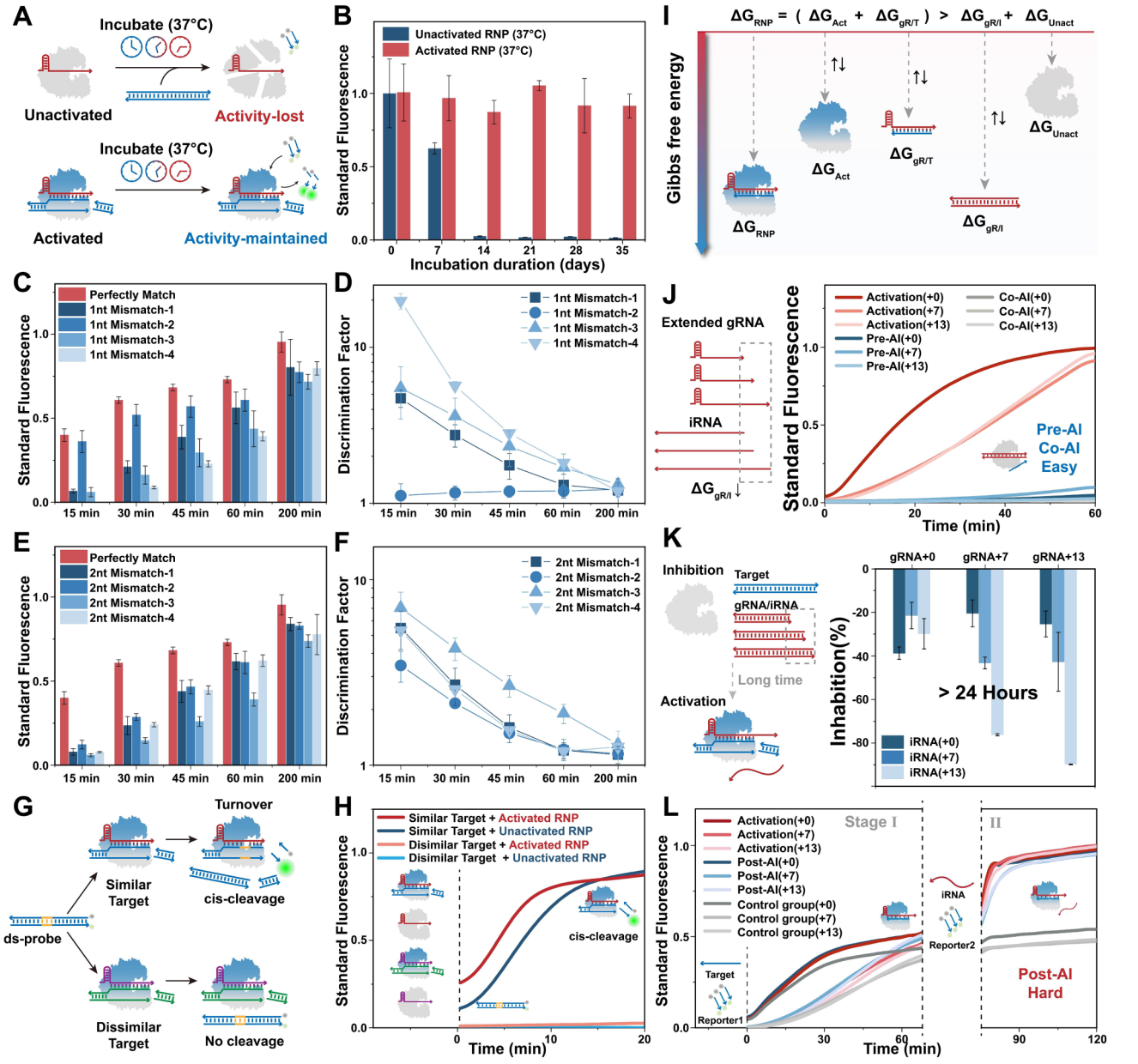


Figure 1. The activity changes of activated and unactivated Cas12a RNPs during 35 days incubation at 37°C and their fluorescence signals (**A, B**); fluorescence kinetics and discrimination factors (DFs) for targets containing 1 nt (**C, D**) or 2 nt (**E, F**) mismatch at different positions; fuzzy recognition and turnover cleavage of Cas12a RNPs evaluated using the ds-probe (**G, H**); thermodynamic relationships of restoring activated Cas12a RNPs to the unactivated state (**I**); enhancement of Pre-AI and Co-AI by extending the gRNA (**J**); inhibition efficiencies after 24 h for gRNAs containing different toehold lengths (**K**); fluorescence kinetics of fully activated gRNAs with different toehold lengths in Stage I and their Post-AI in Stage II (**L**).

could terminate CRISPR activity before loss of control accumulates and, importantly, would be particularly valuable precisely because the activated state is both persistent and intrinsically difficult to reverse.

The theoretical mechanism of iRNA mediated Post-AI

Enthalpy based control of strand displacement reactions (Pre-AI and Co-AI)

From a thermodynamic perspective, the activated state of the Cas12a RNP is highly stable, and restoring it to the unactivated state using iRNA requires providing a lower Gibbs free energy. As shown in Fig. 1I, the Gibbs free energy of the activated RNP (ΔG_{RNP}) can be approximated as the sum of the Gibbs free energy of activated Cas12a (ΔG_{Act}) and that of the gRNA/Target complex ($\Delta G_{gRNA/T}$). For Post-AI to occur, the final products, the gRNA/iRNA complex ($\Delta G_{gRNA/I}$) and unactivated Cas12a (ΔG_{Unact}), must together have a lower Gibbs free energy than ΔG_{RNP}. Based on this, adjusting the free energy differences among the nucleic acid and protein components of the Cas12a RNP can make Post-AI thermodynamically feasible.

Toehold-mediated strand displacement (TMSD) [51] is a classic programmable reaction in dynamic nucleic acid nanotechnology: an invading strand binds to a single-stranded toehold region on a duplex complex and initiates base by base branch migration, ultimately displacing the shorter strand

Downloaded from https://academic.oup.com/nar/article/54/8/gkag436/8666736 by guest on 05 May 2026

completely. This reaction always proceeds toward forming more base pairs, and its yield is strongly influenced by toehold length. This is because a toehold enables the reaction product to form additional base pairs and thus more hydrogen bonds ($\Delta H < 0$), resulting in a negative Gibbs free energy change ($\Delta G = \Delta H - T\Delta S < 0$), which drives the reaction forward. According to the thermodynamic principles of TMSD, increasing the free-energy difference between the reactants and products of iRNA strand displacement requires an appropriately long toehold to increase the number of base pairs in the product.

To decrease $\Delta G_{gRNA/I}$ of the gRNA/iRNA complex, we extended the 3′ end of the gRNA by 7 or 13 nt and designed corresponding iRNAs complementary to these extensions. As shown in Fig. 1J, extending the gRNA only slightly reduced the *trans*-cleavage rate of Cas12a RNP (Activation + 0/+7/+13), and the reporter was still completely cleaved within 60 min, indicating that the extension had minimal interference with the intrinsic performance of Cas12a RNP. On the other hand, adding iRNA to the reaction mixture before target activation (pre-activation inhibition, Pre-AI + 0/+7/+13) or simultaneously with the target (competitive-activation inhibition, Co-AI + 0/+7/+13) both significantly blocked CRISPR/Cas12a activation by the target (Supplementary Scheme S1). In this experiment, the gRNA + 0 group contained no toehold but still achieved Pre-AI and Co-AI, likely because the secondary structure at the 5′ end of the gRNA (the handle region) could be linearized by iRNA, forming additional base pairs and providing a thermodynamic advantage. Nevertheless, the contribution of the toehold remains meaningful. As shown in Fig. 1K, after 24 h of incubation with the target, the inhibitory effect of Pre-AI began to weaken: the gRNA + 0 group showed the poorest inhibition (−20.4%), whereas the gRNA + 13 group with the longest toehold maintained nearly complete inhibition (−89.9%).

Although the thermodynamic principles of TMSD are well reflected in iRNA mediated Pre-AI and Co-AI, applying this strategy to the focus of this study, Post-AI of Cas12a RNP, encountered difficulty (Supplementary Scheme S1). As shown in Fig. 1L, we divided the reaction into two stages. In Stage I, we directly added the target to activate Cas12a RNP (+0, +7, +13) until reporter 1 was completely cleaved, ensuring that all Cas12a RNPs were fully activated. Before Stage II, we added an additional reporter 2 (control group received none) along with iRNAs (+0, +7, +13) (only in the Post-AI groups) to evaluate Post-AI effects. The results showed that reporter 2 was rapidly cleaved by the activated RNPs (activation and Post-AI groups), and iRNAs (+0, +7, +13) had almost no effect. This was unexpected, because extending the toehold should thermodynamically favor iRNA strand displacement and had indeed enabled strong Pre-AI and Co-AI effects; however, it had almost no impact on Post-AI. These results suggest that the strong structural stability of activated Cas12a RNPs imposes an additional barrier to iRNA strand displacement.

Regulating the stability of Cas12a RNPs (single-stranded Post-AI)

Prior to activation, the binding between Cas12a and gRNA primarily relies on electrostatic interactions and the secondary structural features of the handle region [1–5]. The overall stability of the complex is relatively weak, and the thermodynamic driving force of TMSD is sufficient to achieve Pre-AI and Co-AI. However, after Cas12a RNP binds to the target, the protein undergoes a characteristic conformational rearrangement: the REC1/REC2 domains rotate extensively and move toward the Nuc lobe, the bridge helix and RuvC domain cooperatively rearrange, and the nucleic acid binding channel progressively closes and tightly clamps the forming R-loop until reaching the locked state [2, 5]. This series of allosteric transitions converts the Cas12a RNP into a highly stable activated ternary complex, forming an extensive and strong protein–nucleic acid interaction network. Therefore, to reverse the activated state of Cas12a, iRNA must not only possess a thermodynamic advantage in nucleic acid pairing but also overcome the substantial energetic barrier imposed by the activated conformation. Based on this, we next attempted to weaken the stability of activated Cas12a RNP to amplify the thermodynamic driving force of iRNA strand displacement.

As shown in Fig. 2A, while keeping the number of base pairs in the gRNA/Target complex unchanged ($\Delta G_{gRNA/T}$ remains nearly constant), we shifted the target toward the 3′ end of the gRNA (+13), exposing the PAM-proximal region of the gRNA as a flexible single-stranded structure. This single-stranded region cannot form stable contacts with the key recognition domains of Cas12a, thereby weakening the stability of the ternary complex (ΔG_{Act} less negative). We define the 3′-end single-stranded extension of the gRNA as the forward toehold (+) and the PAM-proximal single-stranded region as the reverse toehold (−), and systematically compared Post-AI effects under different toehold lengths (−n nt | +m nt). As shown in Fig. 2B–E, when the target was shifted by 1, 2, 3, or 4 nt, the activation efficiency of Cas12a RNP was almost unaffected (fully activated in Stage I); however, upon addition of iRNA in Stage II, the cleavage rate of reporter 2 in the Post-AI group decreased significantly. By comparing the area under the curves and percentage differences among the activation, Post-AI, and control groups, we found that the larger the target shift, the more pronounced the Post-AI effect (22.4%–98.5%). However, when the target was shifted by 5 nt (–5 nt | +8 nt) (Fig. 2F), although the Stage II Post-AI effect remained strong (99.6%), the activation efficiency in Stage I dropped dramatically, indicating that the Cas12a RNP could no longer stably enter the activated state. Overall, moderate target shifting can weaken the stability of activated Cas12a RNP by exposing the reverse toehold region and thereby enhance Post-AI, whereas excessive destabilization impairs proper Cas12a activation.

Next, as shown in Fig. 2G, we divided the extended gRNA into three parts—the handle region (a), spacer region (b), and tail region (c)—to evaluate the Post-AI effects of different types of iRNAs (ab/bc/abc). As shown in Fig. 2H, using a target shifted by 4 nt (−4 nt | +9 nt) as an example, iRNA (abc) exhibited the strongest inhibition (−95% when the tail was 7 nt, and −98% when the tail was 13 nt). Moreover, the inhibitory effect of iRNA could be further tuned by concentration (Fig. 2I). Combined with different iRNA types, target types, and toehold lengths, this strategy enables multidimensional regulation of Post-AI.

The introduction of a reverse toehold can significantly weaken the stability of single-stranded activation of Cas12a RNP, thereby enabling efficient Post-AI. However, the activation mechanisms of single-stranded and double-stranded targets differ fundamentally, making this strategy difficult to directly apply to double-stranded activation. Activation of double-stranded targets depends on PAM recognition by

Downloaded from https://academic.oup.com/nar/article/54/8/gkag436/8666736 by guest on 05 May 2026

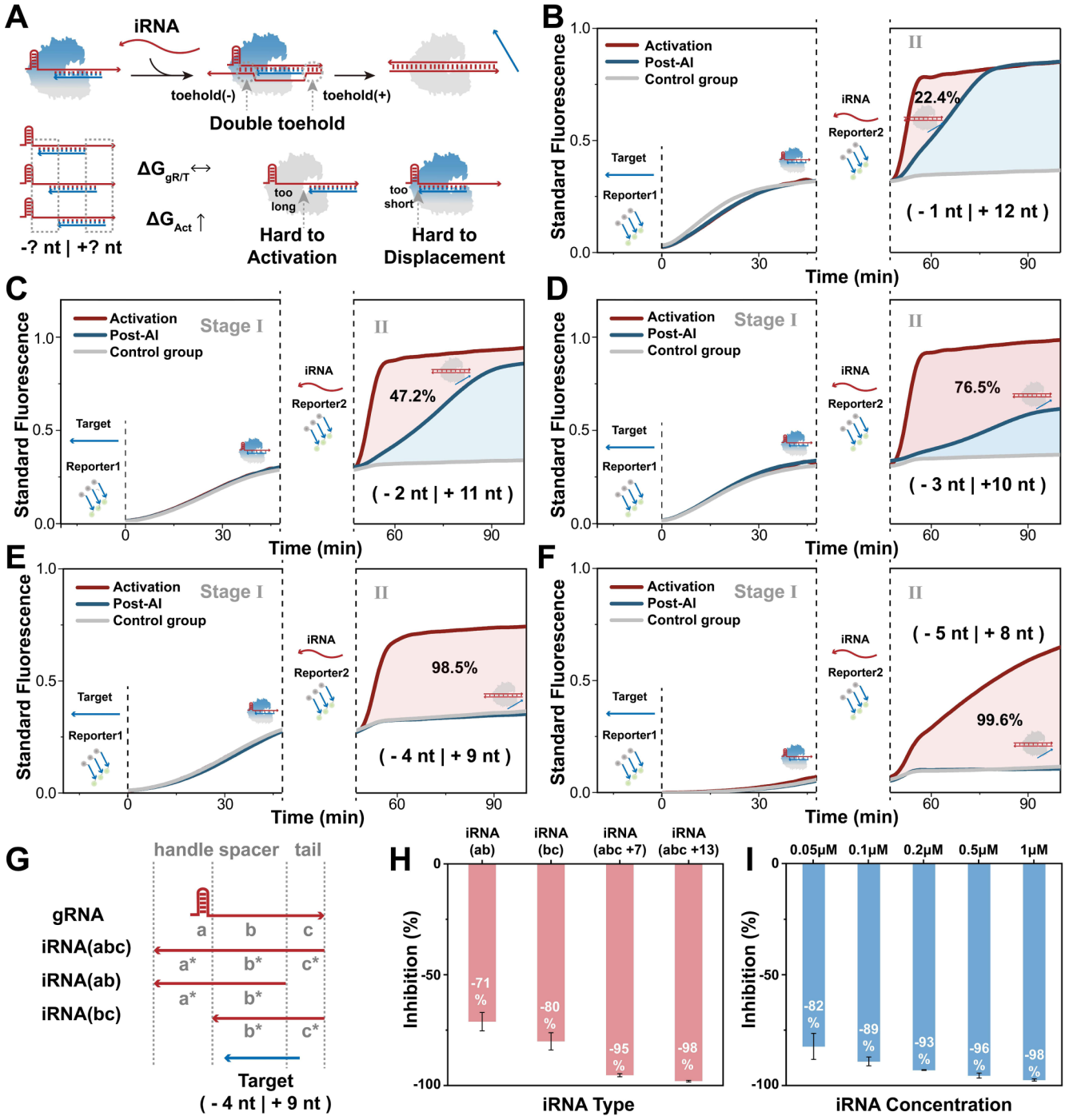


Figure 2. Regulation of Post-AI of Cas12a RNPs by introducing a reverse toehold (**A**); fluorescence kinetics of Cas12a RNPs fully activated in Stage I and inhibited in Stage II with reverse toehold lengths of 1 nt (**B**), 2 nt (**C**), 3 nt (**D**), 4 nt (**E**), and 5 nt (**F**); schematic diagrams for different iRNAs (**G**); Post-AI efficiencies of different iRNA types (**H**) and concentrations (**I**).

Cas12a and the subsequent formation of the R-loop; during this process, bases in the seed region (the PAM-proximal 5–7 nt) must pair strictly to ensure smooth R-loop propagation and eventual triggering of Cas12a conformational rearrangement. Therefore, any shift or base deletion near the PAM-proximal region severely disrupts activation efficiency. This contrasts sharply with single-stranded targets: as shown in Supplementary Fig. S7, single-stranded targets still retained most activation efficiency after shifting by 1, 2, 3, or 4 nt, whereas double-stranded targets lost nearly all activation ability once shifted by only 2, 3, or 4 nt, and even a 1 nt shift required 150 min for partial activation (Supplementary Fig. S8).

Regulating the stability of Cas12a RNPs (double-stranded Post-AI)

Double-stranded DNA is the predominant genetic form in the genome and is also the primary substrate for CRISPR/Cas12a in genome editing and diagnostics [5]. As demonstrated above, increasing the number of base pairs between iRNA and gRNA ($\Delta G_{gRNA/I}$ more negative) and weakening the stability of the

Downloaded from https://academic.oup.com/nar/article/54/8/gkag436/8666736 by guest on 05 May 2026

activated RNP (ΔG_{ACT} less negative) are effective strategies for achieving Post-AI. However, activation of double-stranded targets is extremely sensitive to mismatches within the seed region, making it impossible to directly apply the reverse toehold approach. Therefore, a method is needed that does not disrupt the seed region but can still reduce the stability of the activated state.

To this end, we divided the spacer recognition region into four positions (site 1/2/3/4, progressively closer to the seed region) and introduced mismatches or bulge-loops of different lengths (1/2/3/4 nt) at each position to create localized "instability points" in the target structure (Fig. 3A and B; the sequences in Supplementary Scheme S10). We then systematically evaluated their activation efficiency in Stage I (Fig. 3C–F) and their Post-AI capability in Stage II (Fig. 3G–Z).

For mismatches, single-stranded targets were substantially more tolerant (Fig. 3C): mismatch 1–2 nt at all sites had almost no effect on activation; mismatch 3 nt began to impair activation only at site 3; mismatch 4 nt made activation difficult at site 2/3. In contrast, double-stranded targets were much more stringent (Fig. 3D): mismatch 2 nt at site 4 already resulted in activation failure; mismatch 3 nt at site 3/4 could not activate; mismatch 4 nt at site 2/3/4 entirely abolished activation. The specificity of double-stranded activation is clearly stronger, with site 4 (closest to the seed) being the most sensitive.

For bulge-loops, single-stranded targets (Fig. 3E) displayed clear position dependent effects: bulge-loops of all lengths allowed rapid activation at site 1/2/4, whereas activation was severely hindered only at site 3. double-stranded targets (Fig. 3F) exhibited a similar trend at site 3, and as bulge-loop length increased, activation efficiency at site 4 (near the seed) also gradually decreased. These results suggest that for bulge-loop structures, "position" is more decisive than "length" in determining activation success.

Next, we selected targets that were sufficiently activated in Stage I and directly subjected them to Post-AI testing in Stage II. As shown in Fig. 3G–P, mismatch 1/2/3/4 nt at site 1 produced progressively stronger Post-AI effects (23.9%–90.2%), whereas mismatch 2/3 nt at site 2 exhibited the most pronounced inhibition (96.5%). Likewise, as shown in Fig. 3Q–Z, bulge-loops of different lengths at site 1 produced almost no Post-AI, but at site 2, inhibition efficiency increased proportionally with bulge-loop length (70.0%–94.6%).

In summary, introducing mismatches and bulge-loops allowed us to weaken activated RNP stability (ΔG_{ACT} less negative) while maintaining double-stranded activation efficiency, thereby enabling Post-AI for double-stranded substrates. Notably, altering mismatch length changes the number of matched base pairs and thus modulates $\Delta G_{gRNA/T}$ in a predictable thermodynamic manner (Supplementary Table S3), meaning that mismatch-mediated Post-AI is consistent with thermodynamic expectations. However, bulge-loops of different lengths theoretically do not change the number of base pairs, yet still produced substantial differences in inhibition efficiency. Moreover, bulge-loops located at different positions exhibit similar free energies (Supplementary Table S4) but completely different inhibitory capabilities. These results indicate that the stability of activated Cas12a is determined not only by conventional nucleic acid thermodynamics but also by local structural perturbations and the geometric presentation of protein–nucleic acid interactions.

Theoretical model based on thermodynamic, kinetic, and structural interactions

Although we have already achieved Post-AI of CRISPR/Cas12a in both single-stranded and double-stranded systems, thermodynamic analysis based solely on nucleic acid strand displacement reactions still cannot fully explain the ability of iRNA to reverse the activated RNP state. As shown in Fig. 4A, in pure nucleic acid systems, binding of iRNA to the single-stranded toehold region is the major rate-limiting step of the TMSD reaction. Typically, when the toehold length exceeds 7 nt, the reaction rate approaches saturation, and the subsequent branch migration process is extremely fast, with each step occurring on the μs–ms timescale. However, in the context of activated Cas12a RNPs (Fig. 4), even if iRNA rapidly binds to the gRNA toehold, the subsequent branch migration must proceed within the highly constrained nucleic acid channel imposed by the activated Cas12a conformation. This process is impeded by the conformational locking of the REC/BH/Nuc domains, causing the reaction rate constant k to decrease dramatically, creating an additional rate-limiting step, thereby making Post-AI difficult to achieve. (The inhibitory effects of iRNA on Pre-AI, Co-AI, and Post-AI modes at different time points are shown in Supplementary Fig. S9.)

We further validated the influence of Cas12a on strand displacement kinetics using fluorescence displacement assays. As shown in Fig. 4C, we modified the 5′ end of the gRNA with a quencher and the 3′ end of the target with a fluorophore. When iRNA successfully displaced the gRNA/Target duplex, a rapid fluorescence signal was produced (only nucleic acid +7, +13). However, upon addition of Cas12a to the reaction system, the displacement efficiency was significantly reduced (with Cas12a +7, +13), and the remaining fluorescence likely resulted from strand displacement occurring only among free nucleic acids. These results indicate that effective Post-AI of Cas12a requires not only rational thermodynamic design but also consideration of how the conformational stability of activated Cas12a affects reaction kinetics. As shown in Fig. 4D, our previously introduced reverse toeholds, mismatches, and bulge-loops are proposed to shift activated Cas12a RNPs toward metastable states, allowing them to retain efficient nucleic acid cleavage while also enabling iRNA to rapidly initiate branch migration (Supplementary Fig. S10), thereby promoting the transition from the activated to the unactivated state on both thermodynamic and kinetic levels.

To further probe the mechanistic model for Cas12a Post-AI, we performed molecular dynamics (MD) simulations and structural visualization analyses for the three strategies (reverse toehold, mismatch, bulge-loop). Details of model construction are provided in the "Materials and methods" section. Binding energies between Cas12a/gRNA and target were calculated using the MM–PBSA (molecular mechanics/Poisson–Boltzmann surface area) method (results from the alternative MM–GBSA and potential-energy analyses are shown in Supplementary Table S5; structural analyses are provided in Supplementary Figs S11–S17).

As shown in Fig. 4E, binding free-energy calculations revealed that, compared with the single-toehold model (0 nt | +13 nt), the reverse toehold model (−4 nt | +9 nt) significantly reduced the binding stability of Cas12a/gRNA to the target (from −311.08 kcal/mol to −206.41 kcal/mol). Structural analysis provided a plausible structural explanation for this affinity change. Electrostatic potential mapping showed

Downloaded from https://academic.oup.com/nar/article/54/8/gkag436/8666736 by guest on 05 May 2026

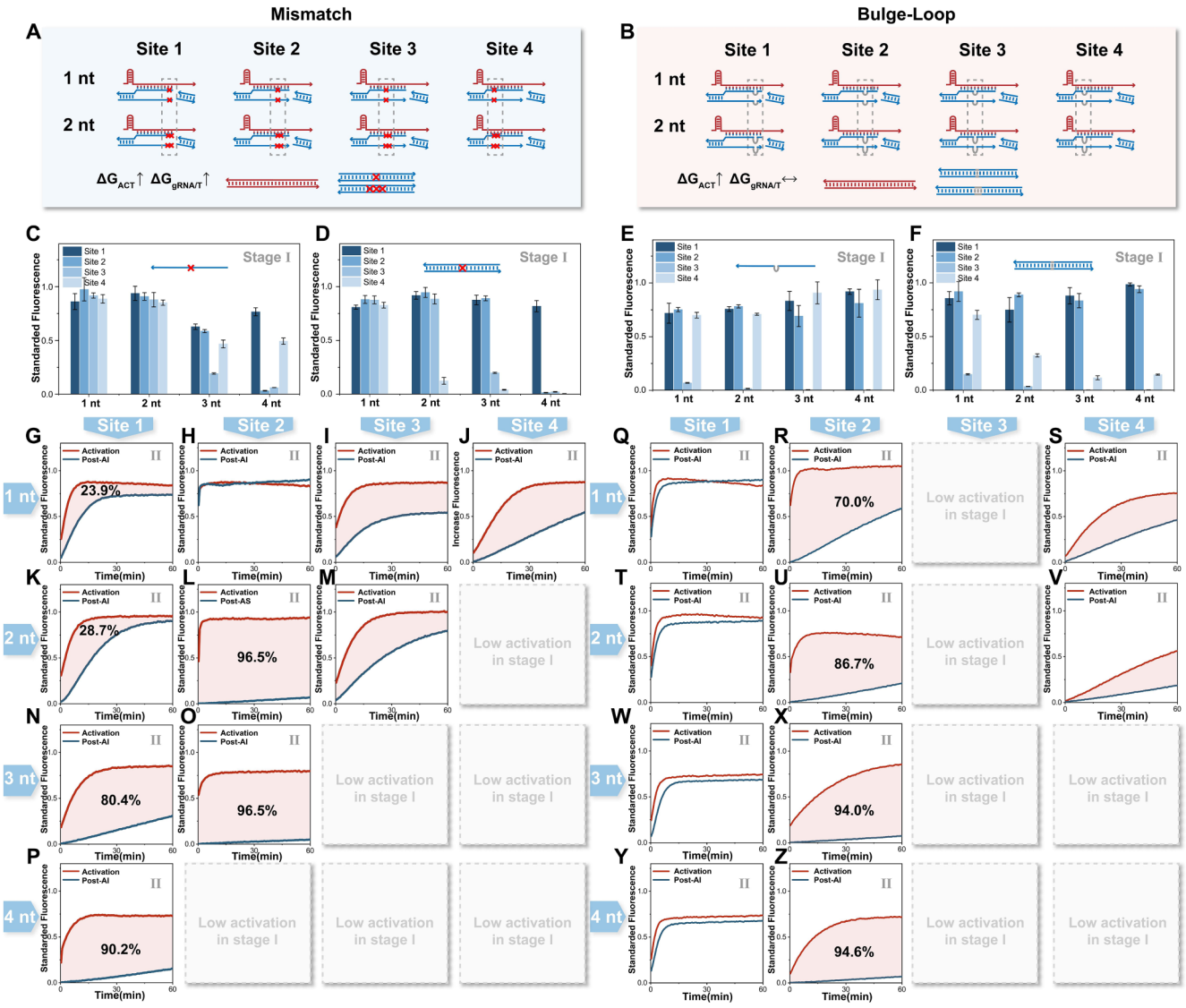


Figure 3. Regulation of Cas12a RNP Post-AI by introducing position-restricted mismatches (**A**) and bulge-loops (**B**); fluorescence signals of Cas12a RNP single-stranded activation (**C**) or double-stranded activation (**D**) with mismatches of different lengths at different positions; fluorescence signals of Cas12a RNP single-stranded activation (**E**) or double-stranded activation (**F**) with bulge-loops of different lengths at different positions; fluorescence kinetics of activated Cas12a RNPs in activation groups and Post-AI groups when mismatches (**G–P**) or bulge-loops (**Q–Z**) of different lengths occur at different positions. Groups that exhibit insufficient activation in Stage I are not suitable for Post-AI evaluation.

that Cas12a contains a prominent positively charged cavity (blue region in the electrostatic surface), which serves as a key site for nucleic acid substrate binding. In the single-toehold RNP model, approximately four paired bases of the gRNA/target duplex precisely occupy the top of this positively charged cavity (within the spatial region formed by the WED and PI domains). These bases form a robust interaction network with surrounding residues, including hydrogen bonds with GLY-783, SER-186, and ASN-178, as well as strong electrostatic attractions with the positively charged LYS-603 and LYS-1054. These multiple interactions effectively anchor the nucleic acid duplex to the protein surface, ensuring tight binding. In contrast, in the double-toehold RNP model, the nucleic acid presentation at this region is altered and can no longer effectively occupy the key positively charged cavity, resulting in markedly weakened interactions. Clustering analysis was then performed on MD trajectories, using the RMSD of protein and nucleic acid snapshots relative to the first frame as the metric. The trajectory was divided into 10 clusters, and the most representative snapshots were selected for structural analysis (Supplementary Figs S18 and S19). These modeled changes suggest that loss of critical interaction sites weakens protein–nucleic acid binding, while the additional binding site introduced by the reverse toehold may render the complex more susceptible to iRNA attack.

For the double-stranded activation mode, Cas12a strictly requires an intact seed region and therefore cannot utilize the reverse toehold strategy to perturb the PAM-proximal structure. Instead, we introduced mismatches or bulge-loops to weaken the binding stability of Cas12a/gRNA and the target. MD simulation results (Fig. 4F–G) showed that a 4 nt mismatch at site 1 is markedly less stable than a 1 nt mismatch (site1-MM1nt = −300.4 kcal/mol, site1-MM4nt = −285.5 kcal/mol), consistent with the experimental trends in Fig. 3G–P: more mismatch bases correspond to lower RNP stability. For the same 4 nt mismatch, instability was even

Downloaded from https://academic.oup.com/nar/article/54/8/gkag436/8666736 by guest on 05 May 2026

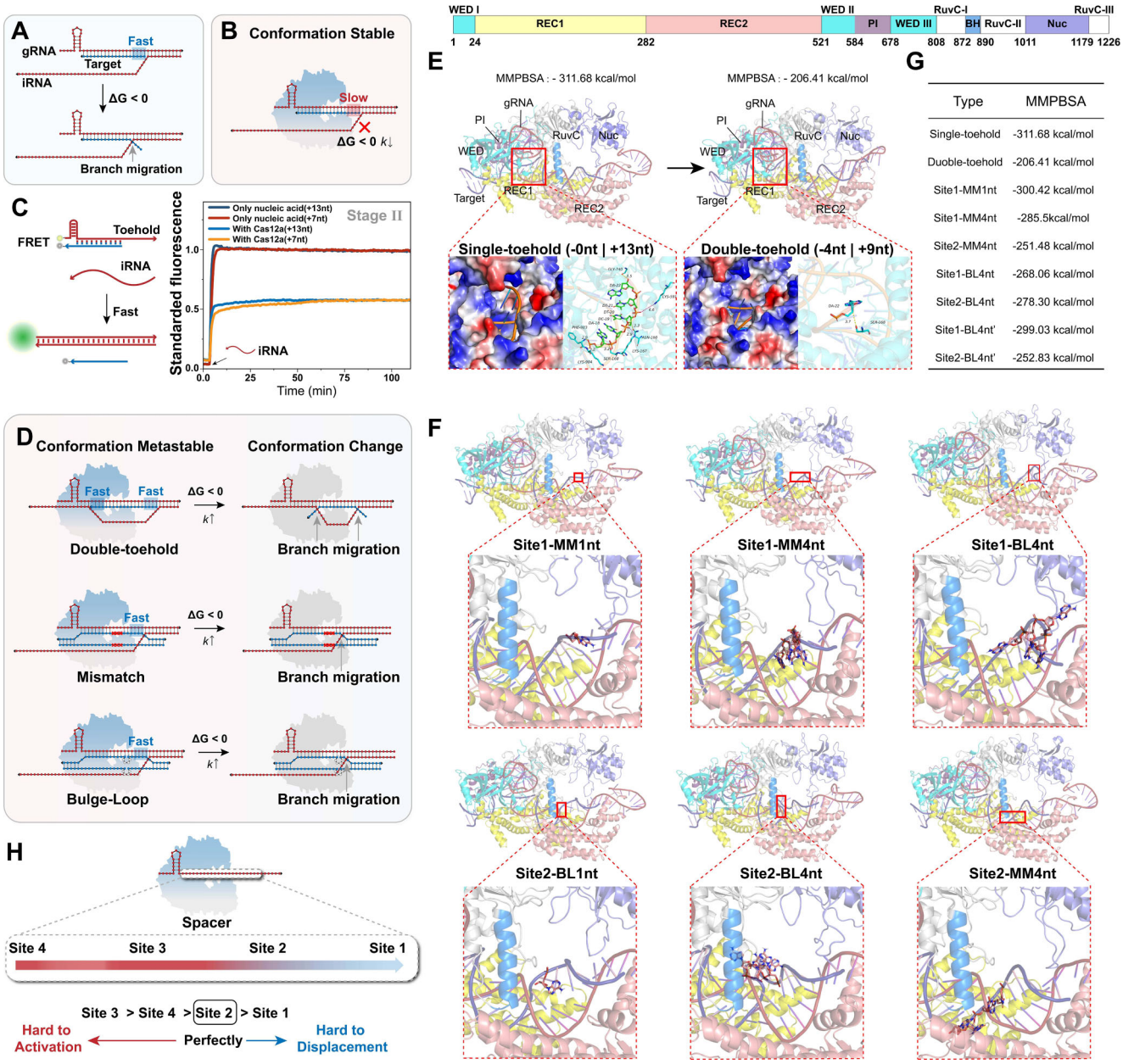


Figure 4. Direct TMSD reactions between iRNA and gRNA/target (**A**) and TMSD reactions occurring on activated Cas12a (**B**); the fluorescence result of iRNA strand displacement in the presence or absence of Cas12a (**C**); metastable activated Cas12a RNP conformations in double-toehold, mismatch, and bulge-loop models that facilitate iRNA strand displacement (**D**); binding free energy analysis, molecular structural analysis, and electrostatic-potential surface analysis of single-toehold and double-toehold models (**E**); representative conformations of mismatch and bulge-loop models of different positions and lengths (**F**); MMPBSA data for each model (**G**); sensitivity of instability points occurring at different positions within the spacer (**H**).

greater at site 2 (site2-MM4nt = −251.48 kcal/mol), because structurally, site 1 is mostly exposed to solvent, whereas site 2 is closer to the REC1/REC2 interface and therefore more likely to affect protein–nucleic acid interactions (Fig. 4F). This may help explain why site2-MM4nt exhibits such low stability that activation becomes difficult (Fig. 3D). For 4 nt bulge-loops, results at site 1 and site 2 initially appeared opposite, this discrepancy is likely due to transient and artificial bulge-residue contacts occasionally formed during unconstrained MD. After removing these artifacts, the corrected values matched the experimental results in Fig. 3Y–Z, supporting the interpretation that bulge-loops at site 2 exert a stronger destabilizing effect on the RNP than those at site 1 (site1-BL4nt′ = −299.0 kcal/mol, site2-BL4nt′ = −219.4 kcal/mol).

Unlike mismatches (Fig. 3G–P), increasing bulge-loop length at site 1 did not produce Post-AI (Fig. 3Q–Y). Comparing the site1-MM4nt and site1-BL4nt models (Fig. 4F), we found that increasing mismatch length at site 1 expands its influence into adjacent positions, gradually approaching the more critical site 2. In contrast, increasing bulge-loop length at site 1 affects only the local region (site 1 alone). Similarly, the influence of site2-MM4nt spreads into the highly sensitive site 3, making Cas12a RNP activation difficult (Fig. 3D), whereas the influence of site2-BL4nt remains confined to site 2, weak-

Downloaded from https://academic.oup.com/nar/article/54/8/gkag436/8666736 by guest on 05 May 2026

ening stability without impairing activation and thereby producing the optimal Post-AI effect (Fig. 3Z). Thus, instability points generated by mismatches and bulge-loops differ spatially in their ranges of influence.

In summary (Fig. 4H), when the influence of an instability point is confined near site 1, the Cas12a RNP conformation remains sufficiently stable and Post-AI is difficult. When site 2 is affected, the Cas12a RNP adopts a metastable conformation that achieves a favorable balance between activation and Post-AI. When site 3 or site 4 is affected, the RNP conformation becomes unstable, and activation itself is severely impaired. Additional strategies are explored in Supplementary Figs S20–S24.

Performance validation and application potential of iRNA mediated Post-AI

High efficiency, versatility, programmability, and expandability

RNA anti-CRISPRs (rAcrs) from bacteriophages and mobile genetic elements, which naturally function to disrupt CRISPR immunity, can also serve as unmodified CRISPR inhibition tools. For example, additional gRNA molecules can, under specific conditions, displace the gRNA within the Cas12a/gRNA complex, and certain small noncoding RNAs can interfere with the CRISPR system by mimicking either the full gRNA or its handle region [6, 12, 42]. However, such strategies inherently rely on structural similarity to the original gRNA and inhibit CRISPR through mimicry-based competitive binding, making them more suitable for pre-activation inhibition or competitive inhibition during activation. For Cas12a RNPs that have already entered the conformationally locked and highly stable activated state, these complexes are difficult to reverse using structural mimicry or passive competition mechanisms (Fig. 5A and Supplementary Fig. S25).

Unlike electrophoresis or other *cis*-cleavage assays, we used the far more amplification-sensitive *trans*-cleavage activity as the evaluation metric for Post-AI, which imposes a stricter requirement. Because Cas12a exhibits extremely strong *trans*-cleavage activity, even a trace amount of uninhibited RNP is sufficient to rapidly cleave the reporter and generate strong fluorescence. As shown in Fig. 5B, when different concentrations of another gRNA or another handle were added before CRISPR/Cas12a activation, the reporter was not *trans*-cleaved, demonstrating strong pre-activation inhibition. However, when these inhibitors were added after Cas12a RNPs were fully activated, the reporter was still rapidly cleaved, indicating almost no Post-AI effect. In contrast, iRNA exhibited substantially higher Post-AI efficiency.

Importantly, whether functioning in pre-activation inhibition or Post-AI, iRNA strand displacement does not disrupt the structure of the Cas12a protein. Instead, it reversibly dissociates the RNP into the protein and nucleic acid components. Thus, the iRNA strategy naturally provides reversibility and strong cyclic activity control, greatly enhancing the safety and programmability of the CRISPR system. As shown in Fig. 5C, adding iRNA on demand immediately terminates Cas12a RNP activity, whereas introducing the same or a different gRNA reassembles the RNP and restores activity. Based on this principle, we achieved cyclic activity control following a "Cleavage/Inhibition/Cleavage/Inhibition/Cleavage" (C/I/C/I/C) process (Fig. 5D): after activation and complete cleavage of reporter 1 (Cleavage in Stage I), adding iRNA induced Post-AI such that reporter 2 was not cleaved (Inhibition in Stage II); adding gRNA and target reactivated the system and rapidly cleaved reporter 2 (Cleavage in Stage III); adding iRNA again prevented cleavage of reporter 3 (Inhibition in Stage IV); and finally, adding gRNA and target once more reactivated Cas12a RNP and rapidly cleaved reporter 3 (Cleavage in Stage V). In comparison, when iRNA was absent, Cas12a RNP remained highly active throughout all five stages, and reporter 2 and reporter 3 were immediately cleaved upon addition in Stage II and Stage IV, respectively (Fig. 5E–G). As shown in Fig. 5H, the calculated cleavage rates indicate that all systems cleaved reporter 1 in Stage I, but the C/I/C/I/C system cleaved reporter 2 only in Stage III and reporter 3 only in Stage V. Moreover, the cleavage rates of reporter 2 and reporter 3 in the C/I/C/I/C system were markedly slower than in the other systems yet comparable to the cleavage rate of reporter 1, confirming that the other systems exhibited continuous Cas12a activity, whereas the C/I/C/I/C system underwent complete shutdown and subsequent reactivation.

Reactivation of Cas12a RNP is not limited to stopping and restoring activity on the same target; it also enables programmable switching across different targets. As shown in Fig. 5I, after completing activation (C1) and inhibition (I1) for Target1, introducing gRNA2/Target2 reactivated the system (C2); following another inhibition (I2), introducing gRNA3/Target3 enabled a third activation event (C3). The effect of iRNA2 and iRNA3 is in Supplementary Figs S26 and S27. Such gRNA/iRNA combination switching provides hot-swappable and dynamically programmable control of CRISPR activity across multiple targets, greatly enhancing the reusability and programmability of the CRISPR system in molecular diagnostics and dynamic gene regulation.

In recent years, equipping CRISPR with additional control interfaces through chemical modifications has become a major research direction. Although our method relies entirely on a single unmodified RNA sequence, allowing safer operation and deeper tissue penetration, iRNA is fully compatible with chemically modified approaches, and combining them can further expand functionality. As shown in Fig. 5J, introducing a photosensitive PC-linker onto iRNA allows UV irradiation to cleave the iRNA after inhibition of activated Cas12a RNP, thereby restoring Cas12a activity. As shown in Fig. 5K, PC-linker modified iRNA exhibited excellent Post-AI [I (PC-linker)], and its inhibition was rapidly reversed upon UV irradiation [C (light)].

In summary, iRNA strand displacement enables substantially higher Post-AI efficiency and, because it does not harm Cas12a, allows robust cyclic activity control. Through combinatorial switching of different iRNAs and gRNAs, highly programmable control can be achieved. Moreover, this strategy leverages the advantages of a completely unmodified system while remaining compatible with chemical modification approaches, offering exceptional expansion potential.

High orthogonality and universality

Direct disruption of Cas proteins or gRNAs can terminate CRISPR activity, but such approaches are often difficult to reverse and, more importantly, globally inactivate all RNPs in the same system. As a result, they cannot achieve locus-level orthogonal regulation in parallel multitarget settings. This is the core problem addressed by the iRNA strategy.

As shown in Fig. 6A, when multiple Cas12a RNPs simultaneously target different genes, disrupting the Cas protein or

Downloaded from https://academic.oup.com/nar/article/54/8/gkag436/8666736 by guest on 05 May 2026

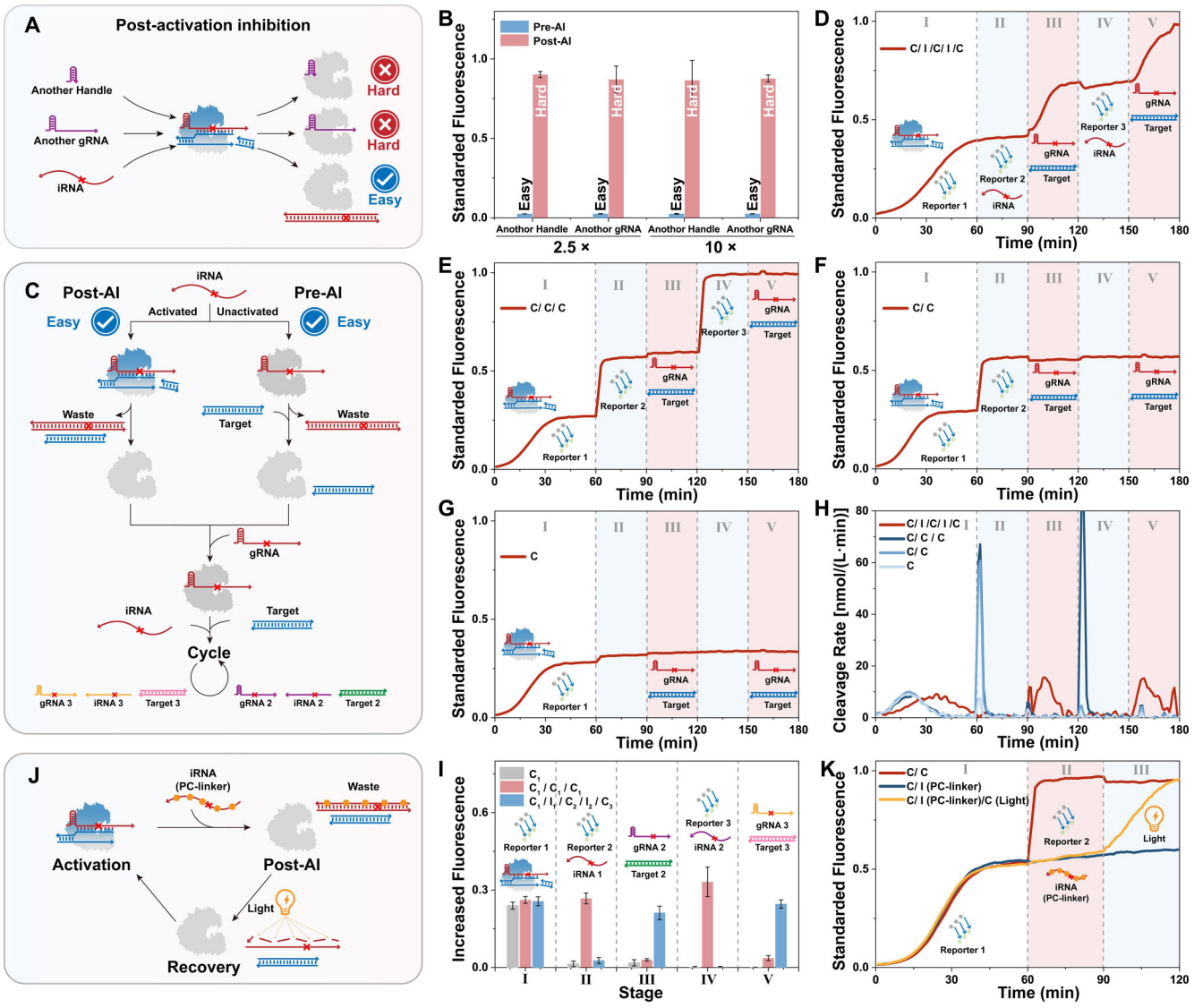


Figure 5. Post-AI is difficult to achieve using another gRNA or another handle (**A**); the Pre-AI and Post-AI effects of another gRNA and handle (**B**); the cyclic activity control (**C**); fluorescence kinetics of Cas12a RNPs across five stages (**D–G**) and their cleavage rates (**H**); controllability and programmability of Post-AI evaluated using different combinations of gRNA, iRNA, and target (**I**); PC-linker-modified iRNA enabling UV-induced cleavage after Post-AI to restore Cas12a RNP activity (**J, K**).

degrading nucleic acid components shuts down the activity of all RNPs at once, preventing selective regulation. Although previous studies have attempted to construct multichannel orthogonal control using photosensitive modifications of different wavelengths, distinct chemical protecting groups, or various stimulus-responsive modules, these strategies often support only a limited number of controllable channels, exhibit poor scalability, and frequently suffer from crosstalk between modules, making it difficult to maintain true orthogonality and universality across different sequence settings in complex systems. In contrast, iRNA inhibition is based on base-by-base strand displacement with gRNA, and recognition is strictly determined by sequence, giving it inherent high specificity, rigorous orthogonality, and strong universality without requiring protein engineering, chemical modification, or stimulus-responsive regulatory modules. For different gRNAs, simply designing the corresponding iRNAs is sufficient to selectively inhibit any designated activated Cas12a RNP among multiple activated complexes without affecting nonmatching RNPs.

As shown in Fig. 6B, after RNP1, RNP2, and RNP3 are fully activated in Stage I, all of them rapidly cleave reporter 2 in Stage II. However, as shown in Fig. 6C, when proteinase K is added in Stage II to digest Cas12a protein, the activity of all RNPs is completely eliminated. Likewise, as shown in Fig. 6D, when RNase If is added in Stage II to degrade gRNAs (Supplementary Figs S28 and S29), each RNP loses all activity. Both approaches lack selectivity and therefore cannot be used for fine regulation in multitarget systems. In contrast, for activated RNP1, RNP2, and RNP3, adding iRNA1 (Fig. 6E), iRNA2 (Fig. 6F), or iRNA3 (Fig. 6G) individually in Stage II results in efficient inhibition only of the matching Cas12a RNP, while the nonmatching RNPs remain completely unaffected, achieving single point selective Post-AI.

Downloaded from https://academic.oup.com/nar/article/54/8/gkag436/8666736 by guest on 05 May 2026

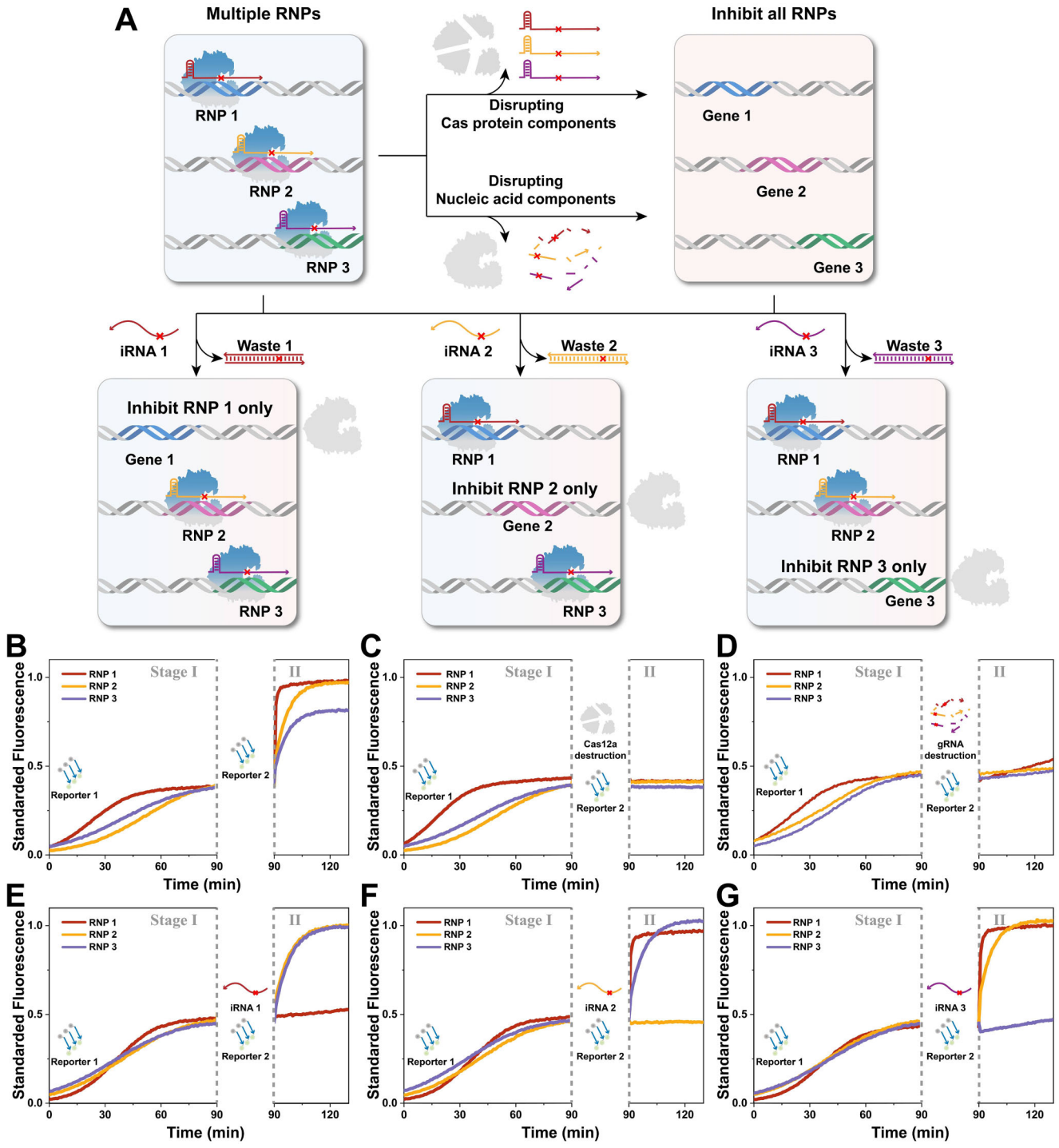


Figure 6. Disrupting Cas protein components or nucleic acid components inhibits all RNPs simultaneously, whereas the iRNA selectively inhibits designated RNPs (**A**); in Stage I, addition of target and reporter 1 fully activates all three RNPs (B–G); in Stage II, adding reporter 2 directly (**B**), or adding after Cas protein degradation (**C**), after gRNA degradation (**D**), after Post-AI by iRNA-1 (**E**), iRNA-2 (**F**), and iRNA-3 (**G**).

The iRNA method is built upon the framework of dynamic nucleic acid nanotechnology, and its inhibitory effect is jointly driven by the thermodynamic advantages of strand displacement, the kinetic properties of the reaction, and the reversibility of the Cas12a activated conformation. Because this mechanism depends entirely on sequence programming, iRNA inherently exhibits high specificity and strict orthogonality, and matching iRNAs can be readily designed for any gRNA sequence. Therefore, it offers exceptional universality and scalability, making it suitable for precise regulation within parallel multitarget systems.

Safety valve in CRISPR genome editing

CRISPR genome editing holds enormous therapeutic potential, but safety issues such as off-target effects, cytotoxicity arising from prolonged activation, and loss of control over

Downloaded from https://academic.oup.com/nar/article/54/8/gkag436/8666736 by guest on 05 May 2026

Cas proteins remain major bottlenecks for clinical translation and practical applications. To evaluate the safety-valve function of iRNA in an actual gene editing context, we first generated a HepG2 cell line stably expressing EGFP through lentiviral transduction (Supplementary Figs S30 and S31), and used EGFP as the target gene for CRISPR editing. Unexpectedly, gRNAs targeting EGFP (gRNA-a, gRNA-b, gRNA-c) caused a pronounced reduction in cell number after transfection (Supplementary Fig. S32), suggesting that EGFP may have been randomly integrated at multiple genomic loci during lentiviral insertion, resulting in simultaneous cleavage at several sites and subsequently inducing severe CRISPR misediting and cytotoxicity. Interestingly, this loss-of-control editing phenotype provided an ideal system for evaluating the safety-valve capability of iRNA.

We first designed iRNA-a (Supplementary Fig. S33), which efficiently inhibits activated Cas12a RNP-a. As shown in Fig. 7A and B, in EGFP stable HepG2 cells, transfection with Cas12a together with gRNA-a induced strong cytotoxicity; however, subsequent addition of the corresponding iRNA-a immediately terminated Cas12a activity and allowed the cells to resume normal proliferation. Cells treated with iRNA-a alone exhibited proliferation curves nearly identical to those of the NC group, indicating that iRNA possesses excellent biocompatibility without triggering cellular stress or additional toxicity. Beyond proliferation metrics, Western blot analysis (Fig. 7C) showed that residual cells in the gRNA-a group expressed only slightly reduced levels of EGFP compared with the control group, because cells in which EGFP had been fully knocked out had undergone apoptosis, leaving only a small population of partially edited cells. In contrast, EGFP expression in the gRNA-a/iRNA-a group was nearly identical to that of the control group, further demonstrating that iRNA can effectively block uncontrolled CRISPR editing in cells.

To dynamically assess the Post-AI capability of iRNA, we used an EGFP plasmid (Supplementary Fig. S34) as the target and transfected it into 293T cells in two stages. As shown in Fig. 7D–F, when the EGFP plasmid was introduced in Stage I together with gRNA-a, Cas12a RNP was activated, resulting in a marked decrease in EGFP expression; when the plasmid was introduced again in Stage II, Cas12a RNP remained active and continued to suppress EGFP expression. However, addition of iRNA-a in Stage II inhibited the activated RNP and restored EGFP expression. This two-round plasmid-transfection assay clearly demonstrates that iRNA strand displacement inhibition is a true Post-AI mechanism rather than competitive-activation or pre-activation inhibition.

Next, to verify the orthogonality of iRNA in living cells, we designed two gRNAs (gRNA-a and gRNA-x) and their corresponding iRNAs targeting two distinct regions (the endogenous sequence-a on the plasmid and the inserted sequence-x; Supplementary Fig. S35) of the EGFP plasmid. As shown in Fig. 7G–I, only the matched pairs gRNA-a/iRNA-a and gRNA-x/iRNA-x restored high EGFP expression, whereas the cross-pair combinations (gRNA-a/iRNA-x and gRNA-x/iRNA-a) failed to rescue EGFP expression. This indicates that iRNA strand displacement inhibition exhibits excellent intracellular orthogonality, specificity, and universality. Importantly, the approach is straightforward to design and does not require diverse chemical modifications or stimulus-dependent activation modules to differentiate among RNPs.

Moreover, as shown in Fig. 7J, iRNA can also be autonomously generated inside cells through transcription from a DNA plasmid and still achieve Post-AI (Supplementary Fig. S36A and B). When coupled with gene circuits or controllable transcriptional systems, iRNA expression can even be automated and ratio regulated. By adjusting the copy number of the iRNA (Supplementary Fig. S36C) cassette within the plasmid or varying the transfection cycles, it has the potential to achieve precise regulation of inhibition efficiency, enabling CRISPR editing to acquire self-feedback and self-protection capabilities without the need for external triggers.

Finally, we validated the practical utility of iRNA in a disease-related multitarget gene-editing context. PCSK9 is a key gene regulating cholesterol levels and influencing the risk of atherosclerosis. We selected PCSK9 as the editing target and designed a corresponding gRNA-PCSK9 (Supplementary Fig. S36D and E), which was delivered alongside the cytotoxic gRNA-a (Fig. 7K), to test whether iRNA could selectively suppress the harmful editing branch while preserving the desired PCSK9 edit. Because activated Cas12a RNP-a induces uncontrolled editing and cytotoxicity, cells without iRNA-a could not survive long enough to generate and expand PCSK9-knockout cells. In contrast, when iRNA-a was added, the loss of control by RNP-a was promptly suppressed, enabling cell survival and successful expansion of PCSK9 knockout cells, thereby achieving safe gene editing (Supplementary Fig. S36F and G).

In summary, iRNA can function in living cells as an orthogonal, biocompatible, programmable, and automated safety valve for CRISPR, offering broad potential for clinical translation and applied biotechnology.

Conclusion

Gene editing technologies based on CRISPR/Cas have achieved breakthrough progress over the past decade, yet their broad practical applications remain constrained by persistent safety concerns. To establish a universal and orthogonal safety valve for CRISPR, this study leverages the intrinsic thermodynamic-kinetic principles of nucleic acids, the self-assembly behavior of strand displacement, and the allosteric sensitivity of Cas12a. Building on these features, we demonstrate specific Post-AI of CRISPR/Cas12a without chemical modification or external stimulation, and systematically elucidate its underlying molecular mechanism.

Using nucleic acid strand displacement as the foundation, we introduced reverse toeholds, mismatches, and bulges at defined positions to generate energy differentials and conformational instability points. Without compromising activation efficiency, these perturbations weakened the stability of the activated RNP complex, enabling iRNA to gain both thermodynamic and kinetic advantages during displacement and thereby achieve Post-AI of Cas12a. MD simulations further revealed site-dependent conformational effects and binding-energy differences, validating the structural basis of iRNA-mediated inhibition.

At the application level, we demonstrated that iRNA not only exhibits high inhibition efficiency and programmability *in vitro*, but also effectively suppresses uncontrolled genome editing in cells, restoring cell proliferation and gene expression. In both the EGFP multisite-integration loss-of-control model and PCSK9 gene editing, iRNA displayed robust safety-valve performance, markedly improving the controllability and safety of genome editing. These results indicate that iRNA can support dynamic regulation in experimental systems and

Downloaded from https://academic.oup.com/nar/article/54/8/gkag436/8666736 by guest on 05 May 2026

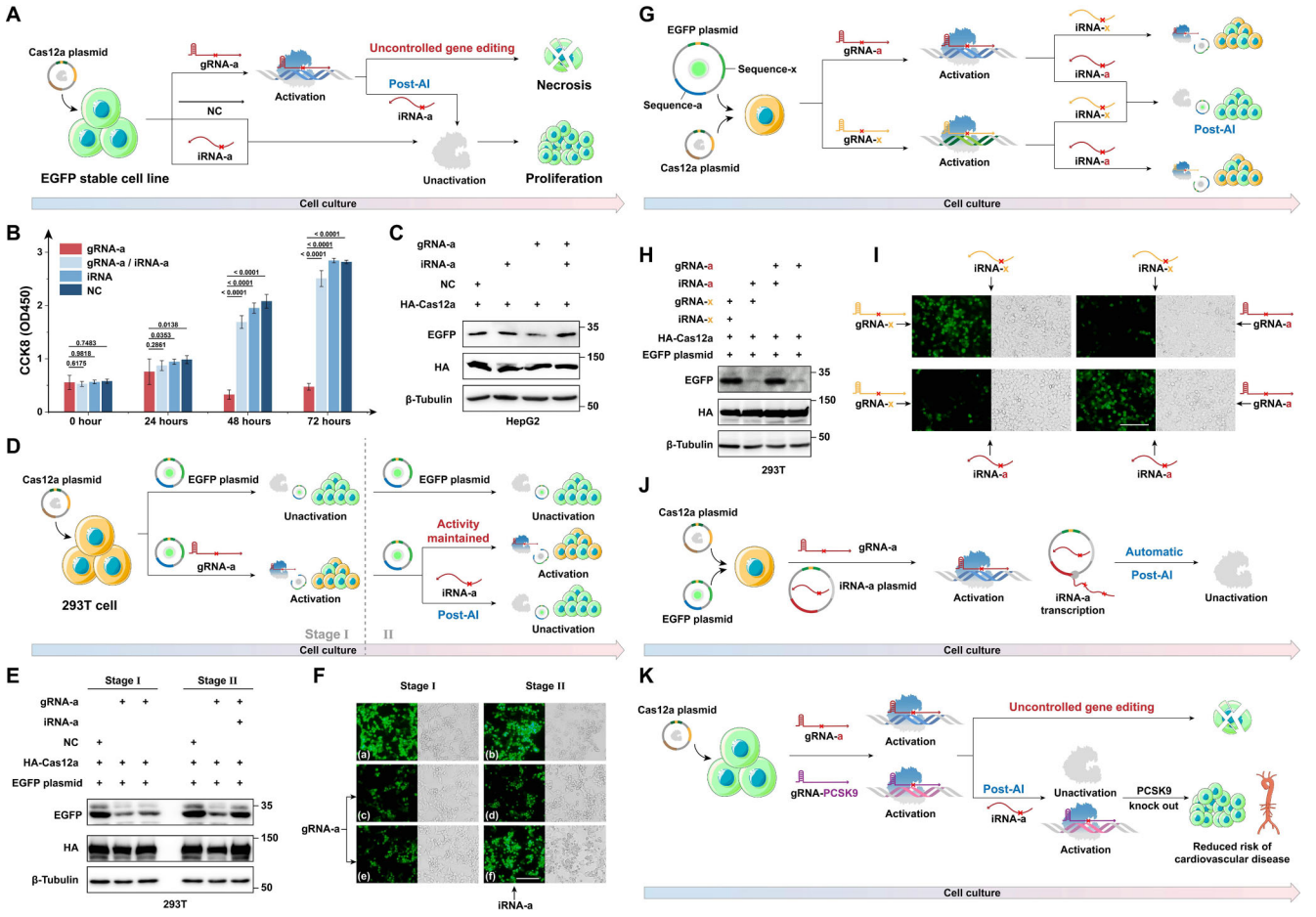


Figure 7. Cytotoxicity induced by uncontrolled genome editing, and the efficacy of iRNA (**A**–**C**); two-stage transfection of EGFP plasmids into 293T cells to test sustained and inhibited Cas12a RNP activity (**D**–**F**); Gene editing through different combinations of gRNAs and iRNAs targeting two EGFP plasmid sequences (**G**–**I**); iRNA produced by plasmid transcription achieving Post-AI (**J**); iRNA selectively suppressing uncontrolled editing and thereby enabling PCSK9 gene knockout in a multitarget setting (**K**). Scale bar, 100 μm.

may also hold promise for *in vivo* therapy and long-term monitoring. However, the "universality" emphasized in this work mainly refers to the design-level generality of the strategy, namely, that it enables regulation without requiring chemical modification, protein engineering, or external stimulation; whether such universality can be further extended across different CRISPR systems still requires further validation and quantitative analysis in other Cas families (such as Cas9 or Cas13) and in broader *in vivo* delivery settings.

In summary, the iRNA strand-displacement inhibition strategy expands the controllability and safety framework of CRISPR systems and provides a foundation for developing higher-level molecular logic regulatory networks, such as self-correction modules for CRISPR. With further integration into gene circuits and controllable transcription systems, iRNA has the potential to become a core component of next-generation adaptive CRISPR systems for precision therapeutics, cell therapy, and molecular diagnostics.

Acknowledgement

Author contributions: Wang Luo (Conceptualization [lead], Data curation [lead], Formal analysis [lead], Funding acquisition [lead], Investigation [lead], Methodology [lead], Project administration [lead], Resources [lead], Software [lead], Supervision [lead], Validation [lead], Visualization [lead], Writing – original draft [lead], Writing – review & editing [lead]), You Wu (Conceptualization [equal], Data curation [equal], Formal analysis [equal], Investigation [equal], Methodology [equal], Resources [equal], Supervision [equal], Validation [equal], Visualization [equal]), Yiqi Zhang (Conceptualization [supporting]), Xiaole Han (Validation [supporting]), Yaoyi Zhang (Supervision [supporting]), Jiu Pu (Formal analysis [supporting]), Weitao Wang (Methodology [supporting]), Yang Sun (Methodology [equal], Project administration [equal], Software [equal], Supervision [equal]), and Guoming Xie (Funding acquisition [lead], Project administration [lead], Resources [lead], Software [lead], Supervision [equal])

Supplementary data

Supplementary data is available at NAR online.

Conflict of interest

None declared.

Downloaded from https://academic.oup.com/nar/article/54/8/gkag436/8666736 by guest on 05 May 2026

Funding

This research work was financially supported by the National Natural Science Foundation of China (82372351, 82572673, 82501041), the Outstanding Project of Chongqing Medical University (BJRC202410), the National Postdoctoral Researcher Support Program (GZC20251421), the Chongqing Natural Science Foundation General Project (CSTB2025NSCQ-GPX1184), the Chongqing National Reserve Talent Program in Health and Wellness (HBRC202404), and the Chongqing Outstanding Youth Science Foundation (CSTB2025NSCQ-JQX0016). Funding to pay the Open Access publication charges for this article was provided by the research grants supporting this study.

Data availability

All data supporting the findings of this study are available within the article and its Supplementary data. Additional information is available from the corresponding authors upon reasonable request.

References

1. Jinek M, Chylinski K, Fonfara I *et al.* A programmable dual-RNA-guided DNA endonuclease in adaptive bacterial immunity. *Science* 2012;337:816–21. https://doi.org/10.1126/science.1225829
2. Knott GJ, Doudna JA. CRISPR–Cas guides the future of genetic engineering. *Science* 2018;361:866–9. https://doi.org/10.1126/science.aat5011
3. Peng W, Shi M, Hu B *et al.* Nanotechnology-leveraged CRISPR/Cas systems: icebreaking in trace cancer-related nucleic acids biosensing. *Mol Cancer* 2025;24:78. https://doi.org/10.1186/s12943-024-02222-5
4. Zhuo C, Zhang J, Lee JH *et al.* Spatiotemporal control of CRISPR/Cas9 gene editing. *Sig Transduct Target Ther* 2021;6:238. https://doi.org/10.1038/s41392-021-00645-w
5. Wang JY, Doudna JA. CRISPR technology: a decade of genome editing is only the beginning. *Science* 2023;379:eadd8643. https://doi.org/10.1126/science.add8643
6. Hayes VM, Zhang J-T, Katz MA *et al.* RNA-mediated CRISPR–Cas13 inhibition through crRNA structural mimicry. *Science* 2025;388:387–91. https://doi.org/10.1126/science.adr3656
7. Sreekanth V, Zhou Q, Kokkonda P *et al.* A molecular glue approach to control the half-life of CRISPR-based technologies. *J Am Chem Soc* 2025;147:23844–56. https://doi.org/10.1021/jacs.5c06230
8. Frock RL, Hu J, Meyers RM *et al.* Genome-wide detection of DNA double-stranded breaks induced by engineered nucleases. *Nat Biotechnol* 2015;33:179–86. https://doi.org/10.1038/nbt.3101
9. Fu Y, Foden JA, Khayter C *et al.* High-frequency off-target mutagenesis induced by CRISPR–Cas nucleases in human cells. *Nat Biotechnol* 2013;31:822–6. https://doi.org/10.1038/nbt.2623
10. Tsai SQ, Zheng Z, Nguyen NT *et al.* GUIDE-seq enables genome-wide profiling of off-target cleavage by CRISPR–Cas nucleases. *Nat Biotechnol* 2015;33:187–97. https://doi.org/10.1038/nbt.3117
11. Sreekanth V, Zhou Q, Kokkonda P *et al.* Chemogenetic system demonstrates that Cas9 longevity impacts genome editing outcomes. *ACS Cent Sci* 2020;6:2228–37. https://doi.org/10.1021/acscentsci.0c00129
12. Camara-Wilpert S, Mayo-Muñoz D, Russel J *et al.* Bacteriophages suppress CRISPR–Cas immunity using RNA-based anti-CRISPRs. *Nature* 2023;623:601–7. https://doi.org/10.1038/s41586-023-06612-5
13. Larsen BB, Kimchi O, Dunkley ORS *et al.* RNA structure modulates Cas13 activity and enables mismatch detection. *Nat Biotechnol* 2025. https://doi.org/10.1038/s41587-025-02868-6
14. Sago CD, Lokugamage MP, Loughrey D *et al.* Augmented lipid-nanoparticle-mediated *in vivo* genome editing in the lungs and spleen by disrupting Cas9 activity in the liver. *Nat Biomed Eng* 2022;6:157–67. https://doi.org/10.1038/s41551-022-00847-9
15. Kang W, Xiao F, Zhu X *et al.* Engineering anti-CRISPR proteins to create CRISPR–Cas protein switches for activatable genome editing and viral protease detection. *Angew Chem Int Ed* 2024;63:e202400599. https://doi.org/10.1002/anie.202400599
16. Liu Y, Liu X, Wei D *et al.* CoHIT: a one-pot ultrasensitive ERA–CRISPR system for detecting multiple same-site indels. *Nat Commun* 2024;15:5014. https://doi.org/10.1038/s41467-024-49414-7
17. Slaymaker IM, Gao L, Zetsche B *et al.* Rationally engineered Cas9 nucleases with improved specificity. *Science* 2016;351:84–8. https://doi.org/10.1126/science.aad5227
18. Kleinstiver BP, Pattanayak V, Prew MS *et al.* High-fidelity CRISPR–Cas9 nucleases with no detectable genome-wide off-target effects. *Nature* 2016;529:490–5. https://doi.org/10.1038/nature16526
19. Zhu Z, Li X, Ding L *et al.* Exploring the effect of activator topology on CRISPR–Cas12a *trans*-cleavage activity. *Nucleic Acids Res* 2025;53:gkaf311. https://doi.org/10.1093/nar/gkaf311
20. Xiao Y *et al.* Cas12a-assisted split crRNA complex for analysis and detection of diverse entities. *Nucleic Acids Res* 2025;53:gkaf1282. https://doi.org/10.1093/nar/gkaf1282
21. Molina Vargas AM, Sinha S, Osborn R *et al.* New design strategies for ultra-specific CRISPR–Cas13a-based RNA detection with single-nucleotide mismatch sensitivity. *Nucleic Acids Res* 2024;52:921–39. https://doi.org/10.1093/nar/gkad1132
22. Chen J, Lin X, Xiang W *et al.* DNA target binding-induced pre-crRNA processing in type II and V CRISPR–Cas systems. *Nucleic Acids Res* 2025;53:gkae1241. https://doi.org/10.1093/nar/gkae1241
23. Han J, Min Y, Hu L *et al.* Tailoring Cas12a functionality with a user-friendly and versatile crRNA variant toolbox. *Nat Commun* 2025;16:8939. https://doi.org/10.1038/s41467-025-64010-z
24. Fu Y, Sander JD, Reyon D *et al.* Improving CRISPR–Cas nuclease specificity using truncated guide RNAs. *Nat Biotechnol* 2014;32:279–84. https://doi.org/10.1038/nbt.2808
25. Economos NG, Quijano E, Carufe KEW *et al.* Antispacer peptide nucleic acids for sequence-specific CRISPR–Cas9 modulation. *Nucleic Acids Res* 2022;50:e59. https://doi.org/10.1093/nar/gkac095
26. Moon J, Zhang J, Guan X *et al.* CRISPR anti-tag-mediated room-temperature RNA detection using CRISPR/Cas13a. *Nat Commun* 2025;16:9142. https://doi.org/10.1038/s41467-025-64205-4
27. Ma L, Lu M, Jia J *et al.* Engineered crRNA for CRISPR/Cas-assisted biosensing. *Trends Biotechnol* 2025;43:8–11. https://doi.org/10.1016/j.tibtech.2024.06.006
28. Hendel A, Bak RO, Clark JT *et al.* Chemically modified guide RNAs enhance CRISPR–Cas genome editing in human primary cells. *Nat Biotechnol* 2015;33:985–9. https://doi.org/10.1038/nbt.3290
29. Sun Y-J, Chen W-D, Liu J *et al.* A conformational restriction strategy for the control of CRISPR/Cas gene editing with photoactivatable guide RNAs. *Angew Chem Int Ed* 2023;62:e202212413. https://doi.org/10.1002/anie.202212413
30. Zhang W, Zhong Y, Wang J *et al.* Direct repeat region 3′ end modifications regulate Cas12a activity and expand its applications. *Nucleic Acids Res* 2025;53, gkaf040.https://doi.org/10.1093/nar/gkaf040
31. Qi Q, Zhang Y, Xiong W *et al.* Norbornene-tetrazine ligation chemistry for controlling RNA-guided CRISPR systems.

Downloaded from https://academic.oup.com/nar/article/54/8/gkag436/8666736 by guest on 05 May 2026

Chem Sci 2022;13:12577–87. https://doi.org/10.1039/D2SC02635J
32. Chen W-D, Liu L, Cheng L. Functionally tunable star-shaped multivalent crRNAs for photocontrol CRISPR/Cas editing. *Angew Chem Int Ed Engl* 2025;64:e202506527. https://doi.org/10.1002/anie.202506527
33. Liu X, Cui S, Qi Q *et al.* G-quadruplex-guided RNA engineering to modulate CRISPR-based genomic regulation. *Nucleic Acids Res* 2022;50:11387–400. https://doi.org/10.1093/nar/gkac870
34. Huang W, Wang J, Wang C *et al.* Expanding Cas12a activity control with an RNA G-quadruplex at the 5′ end of CRISPR RNA. *Adv Sci* 2025;12:2411305. https://doi.org/10.1002/advs.202411305
35. Cai W, Liu J, Chen X *et al.* Orthogonal chemical activation of enzyme-inducible CRISPR/Cas9 for cell-selective genome editing. *J Am Chem Soc* 2022;144:22272–80. https://doi.org/10.1021/jacs.2c10545
36. Cheng Z-H, Luo X-Y, Yu S-S *et al.* Tunable control of Cas12 activity promotes universal and fast one-pot nucleic acid detection. *Nat Commun* 2025;16:1166. https://doi.org/10.1038/s41467-025-56516-3
37. Hu M, Zhang B, Shan Y *et al.* Scalable modulation of CRISPR–Cas enzyme activity using photocleavable phosphorothioate DNA. *Nat Commun* 2025;16:5939. https://doi.org/10.1038/s41467-025-61094-5
38. Li F, Song N, Dong Y *et al.* A proton-activatable DNA-based nanosystem enables co-delivery of CRISPR/Cas9 and DNAzyme for combined gene therapy. *Angew Chem Int Ed* 2022;61,e202116569. https://doi.org/10.1002/anie.202116569
39. Liu H, Dong J, Wu R *et al.* Light-triggered CRISPR/Cas12a for genomic editing and tumor regression. *Angew Chem Int Ed* 2025;64:e202502892. https://doi.org/10.1002/anie.202502892
40. Wu Y, Huang Z, Liu Y *et al.* Ultrasound control of genomic regulatory toolboxes for cancer immunotherapy. *Nat Commun* 2024;15:10444. https://doi.org/10.1038/s41467-024-54477-7
41. Wu J-N, Li C, Liu Z *et al.* Photocontrolled dissociation and toehold-mediated strand displacement-based synergistic regulation of CRISPR–Cas12a. *Nucleic Acids Res* 2025;53:gkaf1178. https://doi.org/10.1093/nar/gkaf1178
42. Stella S, Mesa P, Thomsen J *et al.* Conformational activation promotes CRISPR–Cas12a catalysis and resetting of the endonuclease activity. *Cell* 2018;175:1856–71.e21. https://doi.org/10.1016/j.cell.2018.10.045.
43. Kang X, Yin L, Zhuang S *et al.* Reversible regulation of Cas12a activities by AcrVA5-mediated acetylation and CobB-mediated deacetylation. *Cell Discov* 2022;8:45. https://doi.org/10.1038/s41421-022-00396-0
44. Bi M, Su W, Li J *et al.* Insights into the inhibition of protospacer integration via direct interaction between Cas2 and AcrVA5. *Nat Commun* 2024;15:3256. https://doi.org/10.1038/s41467-024-47713-7
45. Wu Y, Luo W, Weng Z *et al.* A PAM-free CRISPR/Cas12a ultra-specific activation mode based on toehold-mediated strand displacement and branch migration. *Nucleic Acids Res* 2022;50:11727–37. https://doi.org/10.1093/nar/gkac886
46. Zhao R, Luo W, Wu Y *et al.* Unmodificated stepless regulation of CRISPR/Cas12a multi-performance. *Nucleic Acids Res* 2023;51:10795–807. https://doi.org/10.1093/nar/gkad748
47. Cheng X, Li X, Kang Y *et al.* Rapid in situ RNA imaging based on Cas12a thrusting strand displacement reaction. *Nucleic Acids Res* 2023;51:e111. https://doi.org/10.1093/nar/gkad953
48. Ratajczyk EJ, Bath J, Šulc P *et al.* Controlling DNA–RNA strand displacement kinetics with base distribution. *Proc Natl Acad Sci USA* 2025;122:e2416988122. https://doi.org/10.1073/pnas.2416988122
49. Oesinghaus L, Simmel FC. Switching the activity of Cas12a using guide RNA strand displacement circuits. *Nat Commun* 2019;10:2092. https://doi.org/10.1038/s41467-019-09953-w
50. Cohen JC, Boerwinkle E, Mosley TH *et al.* Sequence variations in PCSK9, low LDL, and protection against coronary heart disease. *N Engl J Med* 2006;354:1264–72. https://doi.org/10.1056/NEJMoa054013
51. Zhang DY, Seelig G. Dynamic DNA nanotechnology using strand-displacement reactions. *Nature Chem* 2011;3:103–13. https://doi.org/10.1038/nchem.957

Downloaded from https://academic.oup.com/nar/article/54/8/gkag436/8666736 by guest on 05 May 2026

Received: February 26, 2026. **Revised:** April 15, 2026. **Accepted:** April 16, 2026
© The Author(s) 2026. Published by Oxford University Press.
This is an Open Access article distributed under the terms of the Creative Commons Attribution-NonCommercial License (https://creativecommons.org/licenses/by-nc/4.0/), which permits non-commercial re-use, distribution, and reproduction in any medium, provided the original work is properly cited. For commercial re-use, please contact reprints@oup.com for reprints and translation rights for reprints. All other permissions can be obtained through our RightsLink service via the Permissions link on the article page on our site—for further information please contact journals.permissions@oup.com.